Modulating Antimicrobial Activity and Mammalian Cell Biocompatibility with Glucosamine-Functionalized Star Polymers

Wong, Edgar H. H.; Khin, Mya Mya; Ravikumar, Vikashini; Si, Zhangyong; Rice, Scott A.; Chan-Park, Mary B.

2016

Wong, E. H. H., Khin, M. M., Ravikumar, V., Si, Z., Rice, S. A., & Chan-Park, M. B. (2016). Modulating Antimicrobial Activity and Mammalian Cell Biocompatibility with Glucosamine-Functionalized Star Polymers. Biomacromolecules, 17(3), 1170-1178.

https://hdl.handle.net/10356/83400

https://doi.org/10.1021/acs.biomac.5b01766

Modulating antimicrobial activity and mammalian cell biocompatibility with glucosamine-functionalized star polymers

Edgar H. H. Wong,†[a,b] Mya Mya Khin,[a,b] Vikashini Ravikumar,[c] Zhangyong Si,[a,b] Scott A. Rice[c,d] and Mary B. Chan-Park*[a,b]*

[a.] School of Chemical and Biomedical Engineering, Nanyang Technological University, Singapore 637459.

[b.] Centre for Antimicrobial Bioengineering, Nanyang Technological University, Singapore 637459.

[c.] The Singapore Centre for Environmental Life Sciences Engineering, Nanyang Technological University, Singapore 637551.

[d.] School of Biological Sciences, Nanyang Technological University, Singapore 637551.

ABSTRACT: The development of novel reagents and antibiotics for combating multi-drug resistance bacteria has received significant attention in recent years. In this study, new

antimicrobial star polymers (14-26 nm in diameter) that consist of mixtures of polylysine and glycopolymer arms were developed and were shown to possess antimicrobial efficacy towards Gram-positive bacteria including methicillin-resistant *Staphylococcus aureus* (MRSA) and vancomycin-resistant *Enterococcus* (VRE) (with MIC values as low as 16 μg mL^{-1}) while being non-hemolytic (HC_{50} > 10000 μg mL^{-1}) and exhibit excellent mammalian cell biocompatibility. Structure function analysis indicated that the antimicrobial activity and mammalian cell biocompatibility of the star nanoparticles could be optimised by modifying the molar ratio of polylysine to glycopolymers arms. The technology described herein thus represents an innovative approach that could be used to fight deadly infectious diseases.

INTRODUCTION

The rise of multi-drug-resistance in bacteria is now considered a critical healthcare issue worldwide and the development of alternative antimicrobial agents that kill bacteria by new mechanisms is of paramount importance for overcoming this global healthcare challenge. Hospital-acquired infections such as those caused by Gram-positive pathogens, including the methicillin-resistant *Staphylococcus aureus* (MRSA) and vancomycin-resistant *Enterococcus* (VRE), have resulted in an estimated 23,000 deaths annually in the United States alone.[1] In Europe, MRSA infections affect more than 150,000 patients annually, incurring extra in-hospitable costs worth 380 million EUR per year.[2] Several strategies have been exploited in recent years to identify more effective alternative antimicrobial agents, including the development of the iChip[3] (isolation chip) which allows the screening of soil microorganisms that were previously 'unculturable' in the laboratory. The use of this technology led to the discovery of teixobactin,[4] a highly potent antibiotic in fighting Gram-positive pathogens such as MRSA by inhibiting the bacteria cell wall synthesis. In addition, antimicrobial peptides (AMPs),

which exert their bactericidal properties by physically damaging the bacterial cytoplasmic membrane instead of targeting intracellular targets, has been shown to be effective against a wide spectrum of bacteria.[5,6] However, the synthesis of AMPs usually involve laborious multi-step procedures. In addition, AMPS are generally known to be haemolytic, thus limiting their application.

An alternative approach in the development of new antimicrobial agents lies in the use of synthetic polymer chemistry. Over the last few decades, advances in controlled polymerization has led to a paradigm shift in the widespread application of well-defined synthetic biomaterials using functional macromolecules and nanoparticles produced by techniques such as (*N*-carboxyanhydride (NCA)) ring-opening polymerization (ROP)[7,8] and reversible addition-fragmentation chain transfer (RAFT) polymerization[9] which have found their way into various applications, including drug or gene delivery systems,[10-13] tissue engineering[14,15] and biosensing.[16,17] The ability to efficiently tune the chemical and physical characteristics (such as the functionality, size and shape), and ultimately the biological properties, of the bionanomaterial by simply controlling the polymerization feed compositions and reaction conditions makes polymeric systems highly attractive and applicable in the biomedical field. There are various types of antimicrobial polymer systems that have been previously developed,[18-22] mostly mimicking the amphiphilic feature of AMPs. While these nanomaterials have excellent antimicrobial activity, most are inherently cytotoxic towards human cells, as was observed for, which limits their potential clinical application. Thus, it is essential that the antimicrobial agent is not only effective in combating pathogens but must also demonstrate minimal toxicity towards human cells.

Herein, the development of a new antimicrobial agent with good biocompatibility in the form of glucosamine-functionalized star polymers is described. This star polymer, which is comprised of polylysine and polyglucosamine-based arms radiating from a central cross-linked core, was generated using a combination of various modern synthetic polymer chemistry protocols including RAFT polymerization,[9] NCA-ROP[7] and *click* chemistry.[23-25] The compounds produced exhibited selective killing of Gram-positive over Gram-negative pathogens, were non-haemolytic and exhibited low cytotoxicity towards mammalian cells. The rationale behind the design of this nanoparticle is based on the ability of polylysine to induce bacteria death, whereas the glycopolymer may provide biocompatibility to human cells and the capability to infiltrate the peptidoglycan layer found only in bacteria (because of its resemblance to the peptidoglycan structure). By adjusting the chemical composition, specifically the ratio of polylysine to polyglucosamine-based arms, the antimicrobial activity and mammalian cell biocompatibility can be modulated. It is hypothesized that the star architecture offers a distinct advantage over linear analogues in terms of having better mammalian cell biocompatibility as the polyglucosamine-based arms can effectively shield and reduce the propensity of the cationic polylysine arms from interacting with other cells, thereby decrease cytotoxicity when the arms are 'locked' in a nanoparticle form. The results from the compounds developed here suggest that these compounds represent a structure that can be further modified and optimised for the subsequent development of antimicrobial agents for clinical applications.

EXPERIMENTAL SECTION

Materials. 5-hexyn-1-ol (Aldrich, 96%), triethylamine (Sigma-Aldrich, ≥ 99%), acryloyl chloride (Merck, ≥ 96%), *N*-acetyl-D-glucosamine (Sinopharm Chemical Reagent), acetyl chloride (Aldrich, 98%), sodium azide (Aldrich, ≥ 99%), copper iodide (CuI) (Sigma-Aldrich,

98%), *N,N,N′,N″,N″*-pentamethyldiethylenetriamine (PMDETA) (Aldrich, 99%), anhydrous dimethylformamide (DMF) (Sigma-Aldrich, 99.8%), anhydrous tetrahydrofuran (THF) (Sigma-Aldrich, ≥ 99.9%), benzylamine (Aldrich, 99%), ethylenediaminetetraacetic acid (EDTA) (Sigma-Aldrich, ≥ 99%), *N*-(2-hydroxyethyl)acrylamide (HEAm) (Aldrich, 97%), *N,N'*-methylenebis(acrylamide) (Aldrich, 97%), trifluoroacetic acid (TFA) (Sigma-Aldrich, 99%), thioanisole (Sigma-Aldrich, ≥ 99%), trifluoromethanesulfonic acid (TFMSA) (Alfa Aesar, 98%), hydrazine hydrate solution (Sigma-Aldrich, 78-82%), sodium hydrogen carbonate ($NaHCO_3$) (Vetec, 99%), and magnesium sulfate ($MgSO_4$) (Sigma-Aldrich, ≥97%) were used as received. Chloroform ($CHCl_3$), hexane, ethyl acetate (EtOAc), and diethyl ether (DEE) were purchased from Aik Moh Paints and Chemicals and used as received. Deuterated solvents ($CDCl_3$, DMSO-d_6, D_2O) were obtained from Cambridge Isotope Laboratories and used as received. Lys NCA monomer,[13] *N*-succinimidyl-5-hexynoate,[26] 1-((3-azidopropoxy)carbonyl)ethyl butyl carbonotrithioate,[27] and benzyl dodecyl carbonotrithioate[28] were synthesized according to literature procedures. High-purity water with a resistivity of > 15 MΩ cm was obtained from a Merck Millipore Integral 3 water purification system.

Characterization of synthetic (macro)molecules. ^1H and ^{13}C nuclear magnetic resonance (NMR) spectroscopy were conducted on a Bruker Avance DPX-300 spectrometer using deuterated solvents (obtained from Cambridge Isotope Laboratories) as reference solvents and at a sample concentration of *ca.* 10-20 mg mL^{-1}. Gel permeation chromatography (GPC) was carried out on a Shimadzu liquid chromatography system equipped with a Shimadzu refractive index detector (RID-10A) and two Polargel columns operating at 40°C using DMF (with 1 wt% LiBr) as the eluent at a flowrate of 1 mL min^{-1}. Dynamic light scattering (DLS) and zeta-potential measurements were measured using a Malvern Zetasizer Nano ZS apparatus equipped

with a He-Ne laser operated at 633 nm. All samples were measured at a polymer concentration of 1-3 mg mL^{-1} and at a scattering angle of 173°.

Synthesis of 5-hexynyl acrylate, 1. A solution containing 5-hexyn-1-ol (5.1 g, 50.9 mmol) in THF (200 mL) was degassed with Ar for 45 min at 0°C, prior to the sequential addition of triethylamine (8.5 mL, 61.1 mmol) and acryloyl chloride (4.6 mL, 56.0 mmol). The reaction mixture was allowed to warm to room temperature and stirring was continued for another 5 h. Precipitated urea was filtered off, and the solvent was removed *in vacuo*. The contents were re-dissolved in EtOAc (150 mL) and washed against 0.1 M HCl aqueous solution (75 mL × 2), saturated $NaHCO_3$ solution (75 mL × 2), and brine (75 mL × 2) in the following order. The organic phase was dehydrated over $MgSO_4$, filtered and dried *in vacuo* to give **1** as a pale yellow oil (5.7 g, 37.7 mmol, 74 mol%); ^{1}H NMR (300 MHz, $CDCl_3$, 25°C): δ_H (ppm) = 6.40-6.36 (d, 1H, C*H*H=CH), 6.13-6.06 (dd, 1H, C*H*=CH_2), 5.81-5.79 (d, 1H, CH*H*=CH), 4.18-4.15 (t, 2H, CH_2O-C(=O)), 2.24-2.21 (m, 2H, CH_2-C≡H), 1.95 (s, 1H, -C≡*H*), 1.82-1.75 (m, 2H, -CH_2-), 1.64-1.57 (m, 2H, -CH_2-); ^{13}C NMR (300 MHz, $CDCl_3$, 25°C): δ_C (ppm) = 166.1, 130.5, 128.4, 83.8, 68.7, 63.9, 27.6, 24.9, 18.0.

Synthesis of acrylate-functionalized *N*-acetyl D-glucosamine peracetate monomer, 4. In total, the synthesis of the acrylate-functionalized *N*-acetyl D-glucosamine peracetate required four steps. Firstly, to a 100 mL round-bottom flask containing acetyl chloride (50 mL) was added *N*-acetyl-D-glucosamine (10 g) under strong stirring. The suspension was stirred for 1 day at 25°C in a closed system after which the solids were completely dissolved at the end of the reaction (Caution: HCl fumes evolved during the reaction). $CHCl_3$ (100 mL) was then added to the light brown solution and the mixture was poured into ice water (125 mL) under strong stirring. The organic phase was separated and washed against cold, saturated $NaHCO_3$ solution

(100 mL × 3), dehydrated over $MgSO_4$, filtered, and concentrated *in vacuo*. The crude product was purified by silica gel column chromatography to give **2** as a white solid product (8.2 g, 22.4 mmol, yield = 50 mol%); R_f = 0.286 (hexane/EtOAc = 2/3).

The chloro-functionalized sugar **2** (4.8 g, 13.1 mmol) was dissolved in DMF (80 mL). Sodium azide (6.4 g, 98.3 mmol) was added to the solution and the reaction mixture was stirred at 40°C for 1 day. Insoluble salts were filtered off and the solvent was removed *in vacuo*. EtOAc (100 mL) and water (100 mL) were added to the flask and stirred for 10 min. The organic phase was separated and washed against water (50 mL × 2), dehydrated over $MgSO_4$, filtered, and dried *in vacuo* to give **3** as a white solid product (4.2 g, 11.3 mmol, yield = 87 mol%).

Azido-functionalized sugar **3** (2.9 g, 7.8 mmol) was dissolved in EtOAc (60 mL) and the solution was cooled to 0°C in an ice-water bath and degassed with Ar for 45 min. CuI (300 mg, 1.6 mmol), PMDETA (651 μL, 3.1 mmol) and the synthesized 5-hexynyl acrylate **1** (1.3 g, 8.6 mmol) were then sequentially added to the solution. The reaction mixture was stirred at 25°C under positive Ar atmosphere for 6 h. The solution was then washed with EDTA solution (*ca.* 0.05 M in water, 40 mL × 2), followed by water (40 mL × 2). The organic phase was dehydrated over $MgSO_4$, filtered and concentrated *in vacuo*. The concentrated solution was re-precipitated twice into DEE:hexane 7:3 solvent mixture (100 mL) and dried *in vacuo* to yield **4** as a white sticky solid (3.5 g, 6.7 mmol, yield = 86 mol%); ^{1}H NMR (300 MHz, $CDCl_3$, 25°C): δ_H (ppm) = 7.67 (s, 1H, triazole), 6.76-6.73 (d, 1H, amide), 6.41-6.36 (d, 1H, C*H*H=CH), 6.15-6.06 (m, 2H, C*H*=CH_2 and C*H*-N-N=N overlap), 5.83-5.79 (d, 1H, CH*H*=CH), 5.56-5.49 (t, 1H, sugar ring), 5.25-5.18 (t, 1H, sugar ring), 4.60-4.54 (q, 1H, sugar ring), 4.31-4.04 (m, 5H, CH_2O-C(=O) and –C*H*NH-C(=O) overlap), 2.79-2.75 (m, CH_2-C(=C)N), 2.06 (s, 6H, methyl), 1.75 (s, 6H methyl), 2.06-1.75 (m, 4H, -CH_2CH_2-); ^{13}C NMR (300 MHz, $CDCl_3$, 25°C): δ_C (ppm) = 170.7, 170.6,

169.4, 166.9, 147.8, 130.8, 128.5, 120.4, 85.9, 74.8, 72.3, 68.1, 64.2, 61.8, 53.3, 28.1, 25.5, 25.1, 22.8, 21.4, 20.7, 20.6.

Synthesis of *ω*-RAFT end-group-functionalized linear poly(Z-L-lysine). The synthesis of RAFT-functionalized polypeptide proceeded in two steps via tandem NCA-ROP and copper-mediated *click* chemistry. Firstly, Lys NCA monomer (1.35 g, 4.4 mmol) was dissolved in anhydrous DMF (7 mL) under Ar atmosphere. To this solution was added benzylamine (24 μL, 0.22 mmol in 2 mL anhydrous DMF) and the mixture was stirred at 25°C under positive Ar atmosphere for 1 day. At the end of the ROP process, *N*-succinimidyl-5-hexynoate (260 mg, 2,2 mmol in 4 mL anhydrous THF) was added into the reaction for the *in situ* conversion of terminal amines to alkyne groups. The reaction mixture was stirred for another day prior to repeated precipitation in DEE (100 mL). The alkyne-functionalized polymer was dried *in vacuo* and used directly in the next step (1.21 g, yield = 90 wt%); GPC-DRI (DMF): M_n = 3800 g mol^{-1}, $Đ$ = 1.5.

The alkyne-terminated peptide (840 mg, 0.21 mmol yne) and azido RAFT agent, 1-((3-azidopropoxy)carbonyl)ethyl butyl carbonotrithioate (202 mg, 0.63 mmol), were dissolved in DMF (10 mL), and the solution was purged with Ar for 30 min prior to the addition of CuI (16 mg, 0.08 mmol) and PMDETA (35 μL, 0.16 mmol). The solution was stirred for 3 h at 25°C and under positive Ar atmosphere. The polymer was then precipitated into DEE (100 mL) and the excess RAFT agent remained in the supernatant. The polymer was re-dissolved in $CHCl_3$ (40 mL) and washed with EDTA solution (*ca.* 0.05 M in water, 40 mL × 2), followed by water (40 mL × 2). The organic phase was dehydrated over $MgSO_4$, filtered and concentrated *in vacuo*. The concentrated solution was re-precipitated twice into DEE (100 mL) and dried *in vacuo* to yield the RAFT-functionalized poly(Z-L-lysine) as a yellow solid (620 mg, 69 wt%); GPC-DRI (DMF): M_n = 4100 g mol^{-1}, $Đ$ = 1.6.

General linear polymer formation via RAFT-based photopolymerization. Typically, the (macro)RAFT agent and monomer were dissolved with DMSO in a Schlenk tube where the monomer to solvent (wt/vol) ratio is 1:5. The solution was subjected to three freeze-pump-thaw cycles and lastly backfilled with Ar. The Schlenk tube was then placed in the middle of a self-constructed photoreactor and irradiated for a day. (Near) full monomer conversion (> 90%) was attained in all cases. The LED light source was a commercial strip lighting (300 LEDs, 60W total).

General core cross-linked star polymer formation via RAFT-based photopolymerization. In a similar fashion to the synthesis of linear polymers, the pre-formed macroinitiators and cross-linker *N,N'*-methylenebis(acrylamide) (15 mol eq. with respect to the RAFT group) were dissolved with DMSO in a Schlenk tube where the macroinitiator to solvent (wt/vol) ratio is 1:8. The solution was subjected to three freeze-pump-thaw cycles and lastly backfilled with Ar. The Schlenk tube was then placed in the middle of the photoreactor and irradiated for two days. Full conversion of the vinyl groups was observed. The crude sample was re-precipitated twice into DEE and dried *in vacuo* prior to the removal of protecting groups.

General procedure for removal of protecting groups. The carboxybenzyl groups were first removed, followed by the acetyl groups. Generally, the polymer (*ca.* 3 wt%) was dissolved in TFA followed by the addition of thioanisole and TFMSA (5 mol eq. each with respect to Cbz). The solution was stirred at 0^{o}C for 2 h. The contents were re-precipitated thrice into DEE, washed with DEE, and dried *in vacuo* prior to the next step. For the removal of acetyl groups, the polymer (*ca.* 2 wt%) was dissolved in DMSO followed by the addition of hydrazine (11 mol eq. with respect to the acetyl group) and the solution was stirred at 25^{o}C for 12 h. The polymer was re-precipitated twice into DEE, dried *in vacuo*, re-dissolved in water and further purified using a

Vivaspin Centrifugal Concentrator (molecular weight cut-off 3 kDa). The purified solution was then lyophilized to yield a white fluffy product.

Mammalian cell biocompatibility studies. The mammalian cell biocompatibility study was carried out with human aortic smooth muscle cells (AoSMC, CC-2571 Lonza). Mammalian cells were cultured in 96-well plates from initial inocula of 1×10^5 cells in each well. A graded concentration series of polymer solutions in culture medium was prepared, 200 μL of which was added to the cell cultures. The cells were incubated at 37^{o}C for 24 h, then the culture medium containing polymer was removed and each well was washed with PBS prior to the addition of MTT solution (100 μL, 1 mg mL^{-1} in DMEM; initial MTT solution concentration was 5 mg mL^{-1} in PBS). After another 4 h of incubation, the MTT medium was removed. DMSO (100 μL) was added and the plate was shaken at 100 rpm for 15 min. The cell viability was measured based on the absorbance of each well at 570 nm.

Haemolysis studies. The haemolytic activity was determined against human erythrocytes. Erythrocytes were isolated from freshly drawn human blood (approval number: IRB-2015-03-040). Human blood was drawn directly into K_2-EDTA-coated Vacutainer tubes to prevent coagulation of blood. The blood was stored at 4^{o}C for 1 h and centrifuged at 1000*g* for 10 min to get red blood cells (RBC). RBC were washed with PBS for three times (vortex mixing with PBS and centrifugation at 1000*g* for 10 min to remove supernatant) and RBC were re-suspended to achieve 5% (v/v) in PBS (pH 7.4). Serial dilution was done in sterilized tubes by mixing 60 μL of polymer solution (20,000 μg mL^{-1}) with 60 μL of PBS. Serial dilution of the polymers in PBS was performed followed by the addition of 60 μL of erythrocyte suspension to the polymer solutions. PBS buffer (pH 7.4) was used as a negative haemolysis control and Triton X-100 (1% v/v in PBS) was used as a positive haemolysis control. The tubes containing polymer solution

and erythrocyte suspension were incubated for 2 h at 37°C and 150 rpm in an inoculation shaker. Then, RBC with polymer solutions were centrifuged at 1000*g* for 5 min. The supernatants (60 μL) were then transferred to each well of a fresh microtiter plate (96-well microplate) followed by the addition of 60 μL of PBS and absorbance was determined at 540 nm by using a Tecan InfinitePro series M200 Micro plate Reader. The haemolysis percentage (*H*) was calculated from the following equation:

$$Haemolysis = [(O_p - O_b)/(O_t - O_b)] \times 100\%$$

where O_p is the absorbance for the polymer, O_b is the absorbance for the negative control (PBS), and O_t is the absorbance for the positive control of Triton X-100.

Minimum inhibitory concentration (MIC) determination. Bacteria cells were grown overnight at 37°C in Mueller-Hinton broth (MHB) to mid-log phase and diluted to 10^4 to 10^5 CFU mL^{-1} in MHB. A twofold dilution series of 100 μL of polymer solution in medium was made in 96 well microplates, followed by the addition of 100 μL of the bacterial suspension (10^4 to 10^5 CFU mL^{-1}). The plates were incubated at 37°C for 18-24 h, and the absorbance at 600 nm was measured with a microplate reader (BIO-RAD Benchmark Plus, US). A positive control without polymer and a negative control without bacteria were included. MICs were determined as the lowest concentration that inhibited cell growth by more than 90%.

RESULTS AND DISCUSSION

Overall, the synthesis of the glucosamine-functionalized star polymer nanoparticle can be divided into three key stages: i) synthesis of glycopolymer macroinitiator (**L-pGSA**), ii) synthesis of polylysine macroinitiator (**L-pLYS**), and iii) star formation followed by deprotection (Scheme 1). To synthesize the polyglucosamine-based macroinitiator **L-pGSA**, an

acrylate-functionalized sugar monomer **4** was first made via copper-catalyzed alkyne azide cycloaddition (CuAAC)[23,24] where the premade azido-functionalized *N*-acetyl D-glucosamine peracetate **3** was clicked with 5-hexynyl acrylate **1** to introduce a polymerizable group onto the sugar compound (Figure 1). The ^{1}H NMR spectra in Figure 1 depicts the successful transformation of the sugar precursors into the final acrylate-functionalized sugar monomer **4** where all the functional groups (such as the methine proton of the triazole ring at resonance g', δ_H 7.67 ppm and the vinyl protons at resonances a' and b', δ_H 5.79-6.41) were accounted for. The chemical structure of the acrylate-functionalized glucosamine monomer **4** was further confirmed by ^{13}C NMR analysis (Supporting Information (SI), Figure S1).

The sugar monomer **4** was polymerized using a recently developed RAFT-based photopolymerization technique that enables excellent control over molecular weight and end-group retention even at full monomer conversion.[29,30] The polymerization of **4** was taken to 100% monomer conversion after 24 h and without any further purification (Scheme 1, step v), the glycopolymer (**PGSA**) block was chain extended with a spacer block in a one-pot approach upon the addition of *N*-(2-hydroxyethyl)acrylamide (HEAm) (Scheme 1, step vi). Polymerization of the second block was also taken to full monomer conversion after 24 h. ^{1}H NMR analysis of the glucosamine-based homopolymer **PGSA** and diblock copolymer **L-pGSA** showed the chemical compositions of the polymers as expected (SI, Figure S2 and S3). The targeted (and also obtained) number-averaged degree of polymerization (DP_n) for the glucosamine and HEAm blocks in **L-pGSA** are 30 and 50, respectively. GPC differential refractive index (DRI) chromatograms elucidate the formation of a well-defined glycopolymer **PGSA** with a dispersity ($Đ$) value of 1.2 (SI, Table S1), and the subsequent poly(HEAm) chain extended product, **L-pGSA** (note that L denotes for linear morphology and p indicates that the functional (hydroxyl)

groups are in their protected form), was evident based on the shift in molecular weight distribution to shorter retention time (SI, Figure S4). Noteworthy, the inclusion of a poly(HEAm) spacer block was necessary to ensure a higher macroinitiator-to-star conversion under the current reaction conditions as we have observed poor star formation (< 20%) when no or shorter (DP_n = 20) spacer block was used. HEAm was judiciously chosen for our system as poly(HEAm) are known for their excellent biocompatibility with mammalian cells and low-fouling nature.[31,32]

Meanwhile, the synthesis of the polylysine macroinitiator **L-pLYS** initially entails the NCA-ROP of ε-carboxybenzyl(Z)-L-lysine (Lys NCA) monomer with benzylamine (Scheme 1, step i), followed by *in situ* modification of the amino end-group into clickable terminal alkyne via nucleophilic substitution reaction with *N*-succinimidyl-5-hexynoate (Scheme 1, step ii). The linear alkyne-terminated poly(Z-L-lysine) (**PZLL-yne**) was then converted into a macroRAFT agent (**PZLL-RAFT**) after CuAAC reaction with an azido-functionalized trithiocarbonate RAFT agent (Scheme 1, step iii). Finally, the polymer was chain extended with HEAm via the same RAFT-based photopolymerization as above (Scheme 1, step iv), yielding the polylysine macroinitiator **L-pLYS**. The ^{1}H NMR spectra of **PZLL-RAFT** and **L-pLYS** revealed their anticipated chemical compositions, with **L-pLYS** having *ca.* 15 residues of amino acid and a DP_n of 50 for the poly(HEAm) spacer block (which is the same number of spacer units compared to the **L-pGSA** macroinitiator) (SI, Figure S5 and S6). GPC analysis of **PZLL-yne** and **PZLL-RAFT** however, revealed bimodal distributions (SI, Figure S7), which is not entirely surprising given that PZLL experiences a coil-to-helix transition at around a DP_n of 15 and potentially produces a bimodal distribution as an artefact during GPC analysis. This phenomenon has recently been documented in the literature.[33] The shift in molecular weight distribution after chain extension with HEAm indicated that **PZLL-RAFT** was indeed still active.

For the star formation step, the synthesized macroinitiators were mixed as a cocktail mixture at different molar ratios of **L-pGSA** to **L-pLYS** and subjected to RAFT-based photopolymerization in the presence of a cross-linkable monomer, *N,N'*-methylenebis(acrylamide), for 48 h (Scheme 1, step vii). This approach in forming star polymers, termed the arm-first approach, permits the incorporation of various types of macroinitiators (that go on to form the arms of the star) into a single nanoparticle construct as they converge together during the cross-linking step.[34,35] ^{1}H NMR analysis of the star polymers in Figure S8-S12 (SI) revealed their exact chemical compositional structures (**S-pLYS**, **S-pGSA 25**, **S-pGSA 50**, **S-pGSA 65** and **S-pGSA 100**; where S denotes for star polymer and the number indicates the average mol percentage of glycopolymer arm with respect to the total number of arms). In general, GPC analysis of Figure 2a revealed that the polymerizations were well-moderated, with star polymers having $Đ < 1.7$, except for **S-pLYS** ($Đ = 3.5$) because it contains star-star coupled products, while the estimated average number of arms per star particle (N_{arm}) was between 12 to 19 (Table 1 and SI, Figure S13 and Table S1). Noteworthy, the N_{arm} values represent estimates and not the actual molecular weights and were determined relative to polystyrene standards. Given that the star polymer usually adopts a smaller hydrodynamic volume compared to a linear counterpart of equal molecular weight, the N_{arm} values reported in Table 1 most likely underestimate the actual values.[34a] While the GPC DRI chromatograms in Figure 2a clearly illustrate the evolution of linear macroinitiators into higher molecular weight species, only moderate macroinitiator-to-star conversion values (60-65%) were achieved. The star conversion did not improve even after extended polymerization times (72 h).

There are two possible explanations for the moderate star conversions. We hypothesized that the moderate macroinitiator-to-star conversion is due to steric effects. Both **L-pGSA** and **L-**

pLYS contain bulky side-groups that may have created a steric congestion during star formation, thereby preventing the macroinitiators from fully inserting into the nanoparticle form. Furthermore, some of the PZLL chains adopt α-helix structure and occupy larger hydrodynamic volume than random coil configuration, which adds more steric congestion to the already-sterically-congested system. The addition of the spacer block poly(HEAm) relieved the steric hindrance (*vide supra*) but was insufficient to induce a higher macroinitiator-to-star conversion. Another possible reason is that **L-pGSA** and **L-pLYS** contain some dead chains that were unable to participate in the cross-linking step and hence were 'left behind' as observed via GPC analysis. Although possible, it is unlikely that this reason alone contributed to such star conversion values as the RAFT-based photopolymerization method was previously shown to proceed with high efficiency.[27] We believe that the obtained moderate star conversion values were primarily caused by steric effects, and to a lesser extent due to the contamination of dead chains in **L-pGSA** and **L-pLYS**. It is worth mentioning that although the star polymer samples consist partially of linear polymer impurities, as shown below, the glucosamine-functionalized star polymer samples have significantly different (improved) biological properties compared to linear macromolecules. As a proof of concept, this demonstrates the advantage and difference between star and linear polymers even though the current star production pathway could potentially be further optimized to eliminate any linear polymer impurities to obtain pure star products for better comparison.

Proving that the star polymers truly comprise of mixtures of polylysine and glycopolymers is extremely challenging. However, considering that both **L-pGSA** and **L-pLYS** were composed of identical spacer lengths and types (poly(HEAm)) and used the same family of RAFT agent (trithiocarbonate), it is safe to assume that heteroarm stars were formed and not just mixtures of

two homoarm stars. This is especially true given that controlled radical polymerization is a statistical process. Other studies have indirectly shown the successful formation of heteroarm stars via stimuli-responsive hierarchical self-assembly[34,36] but this method of verification the formation of heteroarm stars is not possible with our system. Nevertheless, the indiscriminate incorporation of various macroinitiators to form heteroarm stars using controlled radical polymerization protocols similar to ours, as demonstrated in these reports, provides strong evidence that heteroarm glucosamine-functionalized stars were formed.

The protecting groups (carboxybenzyl and acetyl) of the star and linear polymers were removed sequentially prior to biological testing (Scheme 1, step viii). Firstly, the carboxybenzyl groups of PZLL blocks were removed in the presence of trifluoroacetic acid, trifluoromethanesulfonic acid and thioanisole, followed by the removal of acetyl protecting groups on the glycopolymer using hydrazine. ^{1}H NMR analysis of the star and linear polymers confirmed the quantitative removal of all protecting groups (including the RAFT groups as indicated by the decoloration of the samples from yellow to white) (SI, Figure S8-12, S14 and S15). The samples were then purified by dialysis and lyophilized. Dynamic light scattering (DLS) distributions of the deprotected star and linear polymers (**S-GSA 25**, **S-GSA50**, **S-GSA 65**, **S-GSA 100**, **L-LYS** and **L-GSA**) are shown in Figure 2b. The average hydrodynamic diameter (d_H) values of the water-soluble stars are *ca.* between 14-26 nm, which are distinctively different to the d_H of the linear macroinitiators ($\leq$ 7.2 nm) (Table 1). The size range of the star polymers was comparable to other star polymers that were made via the arm-first approach. Although the star samples consisted of some linear polymer impurities, the DLS results indicated monomodal distributions. We postulate that the linear impurities in the star samples may be entangled with the star species when dissolved in solution, and hence were not detectable by

DLS. Zeta potential measurements showed that the stars are less cationic with increasing glycopolymer content (with zeta potential (ζ) values decreasing from 33.6 to 8.3 mV), which is expected given that the glucosamine moieties are not as cationic compared to polylysine.

To test the mammalian cell biocompatibility of the star polymers, human aortic smooth muscle cells (AoSMC) were used as a model cell line and the metabolic activity, an indicator of viability, was determined using the MTT assay. At 100 μg mL^{-1}, the cell viability was high (> 80%) for all glucosamine-functionalized star polymers (even for **S-GSA 25** with the lowest degree of glucosamine functionalization) (Figure 3a). **S-LYS** which does not contain any glycopolymer units was cytotoxic. At a higher sample concentration of 500 μg mL^{-1}, the cell viability decreased but improved with higher glucosamine content. The half maximal inhibitory concentration (IC_{50}) values for **S-GSA 25** and **S-GSA 50** were determined to be 337 and 369 μg mL^{-1}, respectively (Figure 3b and Table 2). The trend observed in Figure 3 was correlated with the charge density of the star polymer nanoparticle as polymers with higher zeta potential values were more cytotoxic, most likely because of increased electrostatic interactions with the negatively charged cell surfaces.

An additional experiment was performed to ascertain the effect of the star architecture over mammalian cell biocompatibility. For this, a control sample which is a physical blend of **L-LYS** and **L-GSA** (75:25 molar ratio) that mimics the chemical composition of **S-GSA 25** was subjected to similar MTT assay as above (SI, Figure S16). Interestingly, at 100 μg mL^{-1}, the cell viability of **S-GSA 25** was significantly higher (85%) than the control sample (41%) even though it consists of linear polymers of similar chemical composition. This result highlights the unique property of the star architecture in providing better biocompatibility. When locked in a nanoparticle form, it is hypothesized that the polyglucosamine-based arms shield and reduce the

probability of adjacent polylysine arms from non-specific interactions with cell surfaces, giving the star polymer better human cell biocompatibility over free linear chains. It is worthwhile noting that both **S-LYS** and **L-LYS** were equally cytotoxic towards AoSMC, and the mammalian cell viability only improved with the addition of polyglucosamine-based arms.

The sample concentration at which 50% of red blood cells were lysed, defined as the HC_{50}, was used as the metric for determining the haemolytic activity of the polymers. Remarkably, even at the highest polymer concentration tested (10000 μg mL^{-1}), none of the star polymers were haemolytic, including **S-LYS** which has poor cytocompability with SMC (Table 2). The good haemocompatibility for the star polymers may be attributed to the absence of hydrophobic groups, which are known to be responsible for inducing haemolytic activity.[37,38]

The antimicrobial efficacy of the synthesized nanomaterials against a range of Gram-negative and Gram-positive pathogens was determined based on their minimum inhibitory concentrations (MICs) (Table 2). Polymers that do not contain sugar molecules (i.e., **S-LYS** and **L-LYS**) had good antimicrobial activity against both *Escherichia coli* (Gram-negative) and *Staphylococcus aureus* (Gram-positive), with MIC values between 16-64 μg mL^{-1}. On the other hand, polymers that do not contain cationic polylysine (i.e., **S-GSA 100** and **L-GSA**) were not active against all bacteria tested. Interestingly, the glucosamine-functionalized heteroarm stars selectively killed Gram-positive pathogens and not Gram-negative strains. This level of specificity is most likely attributed to the difference in chemical structure between the two families. For Gram-positive bacteria, a thick peptidoglycan layer constitutes as the outermost layer whereas for the Gram-negative family, the outer membrane consists of a lipid bilayer. Given that the glucosamine moieties on the stars resemble the peptidoglycan structure, we hypothesize that the polyglucosamine-based arms assist the infiltration of the nanoparticles into the Gram-positive

bacteria wall, subsequently enabling the polylysine arms to induce cell death. In contrast, the polyglucosamine-based arms act as 'shields' (*vide supra*) instead of 'infiltrators', which hinder the adjacent polylysine arms from interacting with the Gram-negative bacteria outer membrane, rendering the nanoparticles inactive towards Gram-negative pathogens. The decrease in antimicrobial activity with decreasing polylysine content supports the notion that the polylysine arm is the primary cause of bacteria death. Of note, all of the materials were considered non-active against *Pseudomonas aeruginosa*. **S-LYS**, **S-GSA 25** and **S-GSA 50** were further assessed with more Gram-positive pathogens including *E. faecalis*, and clinical strains MRSA and VRE. These stars were most effective against *E. faecalis*, with MICs between 8-64 μg mL^{-1}. Barring **S-LYS** which is potent against all Gram-positive strains tested, the only heteroarm star that was considered to be effective against MRSA and VRE was **S-GSA 25**, with MICs of 32 and 64 μg mL^{-1}, respectively.

The selectivity (also known as therapeutic index) of the star polymers can be defined as the ratio of HC_{50} to MIC or IC_{50} to MIC. The MIC against *S. aureus* was used as the reference. For HC_{50}/MIC index, **S-LYS** yields the best result (> 417), followed by **S-GSA 25** (> 208), **S-GSA 50** (> 104), and **S-GSA 65** (> 39) in the order of increasing glucosamine functionalization. However, as shown in Figure 3, the cytocompatibility of **S-LYS** with a human model cell line SMC was extremely poor (< 30% at 100 μg mL^{-1}). Amongst the heteroarm stars, **S-GSA 25** showed the best IC_{50}/MIC (7.0). Taking into account both the HC_{50}/MIC and IC_{50}/MIC values, **S-GSA 25** was considered to be the best performing antimicrobial agent that exhibited minimal toxicity to human cells in this study. To get an indication on the selectivity of **S-GSA 25**, its HC_{50}/MIC value was compared to other antimicrobial agents like AMPs. **S-GSA 25** outperforms all the AMPs listed in Table 2 in terms of selectivity. Although the AMPs in general have lower

MIC values than **S-GSA 25**, they inherently suffer from having low HC_{50} (and possibly IC_{50}) values. The good selectivity of **S-GSA 25** thus highlights the attractiveness of using star polymers as effective antimicrobial agents.

CONCLUSIONS

In conclusion, novel glucosamine-functionalized core cross-linked star polymers with polylysine and polyglucosamine-based arms were made via a recently developed RAFT-based photopolymerization technique and the arm-first approach. The glycosylated star polymer nanoparticles (14-26 nm in diameter) demonstrate good cytocompatibility with a model mammalian cell line (human aortic smooth muscle cells), yielding > 80% cell viability. In addition, the star polymer samples show superior biocompatibility compared to free linear polymers as the star architecture provide the platform in shielding the particles effectively from non-specific interactions between the polylysine arms with cell surfaces. Furthermore, the star polymers are non-hemolytic even at 10000 μg mL^{-1}. Antimicrobial studies reveal that the glucosamine-functionalized stars target specifically Gram-positive pathogens and not Gram-negative species, most likely because of the resemblance between the glucosamine moieties with the peptidoglycan layer of the bacteria. The stars were also effective against clinical strains such as MRSA and VRE with MICs as low as 32 μg mL^{-1}. Given the good biocompatibility of the glycosylated stars, they demonstrate excellent selectivity (or therapeutic index), with the most optimum being the star having 25% of polyglucosamine-based arms, **S-GSA 25**. The antimicrobial activity and mammalian cell biocompatibility is tunable depending on the molar ratio of polylysine to glycopolymer arms, where stars with lesser glucosamine functionalization exhibit better antimicrobial efficacy but poorer human cytocompatibility and *vice versa*. This crucially demonstrates that an intricate balance between antimicrobial activity and

biocompatibility needs to be struck to achieve the best biological outcome. The technology described in here could lay the foundation for the development of more advanced antimicrobial agents in the future.

ASSOCIATED CONTENT

Supporting Information.

NMR, GPC, and DLS characterizations as well as biocompatibility studies.
This material is available free of charge via the Internet at http://pubs.acs.org.

AUTHOR INFORMATION

Corresponding Author

* E-mail: edgar.wong@unsw.edu.au

* E-mail: mbechan@ntu.edu.sg

Present Addresses

† Centre for Advanced Macromolecular Design and Australian Centre for Nanomedicine, School of Chemical Engineering, The University of New South Wales, Sydney, NSW 2052, Australia.

Author Contributions

The manuscript was written through contributions of all authors. All authors have given approval to the final version of the manuscript.

Funding Sources

1. Singapore Ministry of Education Tier 3 grant (MOE2013-T3-1-002

2. Singapore NMRC Ministry of Health Industry Alignment Fund Category 2 (MOH IAF CAT Application No. MOHIAFCAT2006).

Notes

The authors declare no competing financial interest.

ACKNOWLEDGMENT

This work was funded and supported by a Singapore Ministry of Education Tier 3 grant (MOE2013-T3-1-002) and a Singapore NMRC Ministry of Health Industry Alignment Fund Category 2 (MOH IAF CAT 2, Application No. MOHIAFCAT2006). S.A.R. and V.R. acknowledge financial support from the Singapore Centre on Environment Life Sciences Engineering, whose research is supported by the National Research Foundation Singapore, Ministry of Education, Nanyang Technological University and National University of Singapore, under its Research Centre of Excellence Programme.

REFERENCES

(1) The White House https://www.whitehouse.gov/the-press-office/2014/09/18/executive-order-combating-antibiotic-resistant-bacteria (accessed November 2015).
(2) Köck, R.; Becker, K.; Cookson, B.; van Gemert-Pijnen, J.; Harbarth, S.; Kluytmans, J.; Mielke, M.; Peters, G.; Skov, R. L.; Struelens, M. J.; Tacconelli, E.; Navarro Torne, A.; Witte, W.; Friedrich, A. W. *Euro Surveil.* **2010**, *15*, pii-19688.
(3) Nichols, D.; Cahoon, N.; Trakhtenberg, E. M.; Pham, L.; Mehta, A.; Belanger, A.; Kanigan, T.; Lewis, K.; Epstein, S. S. *Appl. Environ. Microbiol.* **2010**, *76*, 2445-2450.
(4) Ling, L. L.; Schneider, T.; Peoples, A. J.; Spoering, A. L.; Engels, I.; Conlon, B. P.; Mueller, A.; Schäberle, T. F.; Hughes, D. E.; Epstein, S.; Jones, M.; Lazarides, L.; Steadman, V. A.; Cohen, D. R.; Felix, C. R.; Fetterman, K. A.; Millett, W. P.; Nitti, A. G.; Zullo, A. M.; Chen, C.; Lewis, K. *Nature* **2015**, *517*, 455-459.
(5) Wenzel, M.; Chiriac, A. I.; Otto, A.; Zweytick, D.; May, C.; Schumacher, C.; Gust, R.; Albada, H. B.; Penkova, M.; Krämer, U.; Erdmann, R.; Metzler-Nolte, N.; Straus, S. K.; Bremer, E.; Becher, D.; Brotz-Oesterhelt, H.; Sahl, H. –G.; Bandow, J. E. *Proc. Natl. Acad. Sci. U.S.A.* **2014**, *111*, E1409-E1418.
(6) Mohanram, H.; Bhattacharjya, S. *Antimicrob. Agents Chemother.* **2014**, *58*, 1987-1996.
(7) Deming, T. J. *Nature* **1997**, *390*, 386-389.

(8) Nederberg, F.; Connor, E. F.; Möller, M.; Glauser, T.; Hedrick, J. L. *Angew. Chem., Int. Ed.* **2001**, *40*, 2712-2715.
(9) (a) Moad, G.; Rizzardo, E.; Thang, S. H. *Aust. J. Chem.* **2005**, *58*, 379-410; (b) Moad, G.; Rizzardo, E.; Thang, S. H. *Aust. J. Chem.* **2009**, *62*, 1402-1472.
(10) Cobo, I.; Li, M.; Sumerlin, B. S.; Perrier, S. *Nat. Mater.* **2015**, *14*, 143-159.
(11) Nguyen, T. –K.; Selvanayagam, R.; Ho, K. K. K.; Chen, R.; Kutty, S. K.; Rice, S. A.; Kumar, N.; Barraud, N.; Duong, H. T. T.; Boyer, C. *Chem. Sci.* **2016**, *7*, 1016-1027.
(12) Byrne, M.; Victory, D.; Hibbitts, A.; Lanigan, M.; Heise, A.; Cryan, S. –A. *Biomater. Sci.* **2013**, *1*, 1223-1234.
(13) Lam, S. J.; Sulistio, A.; Ladewig, K.; Wong, E. H. H.; Blencowe, A.; Qiao, G. G. *Aust. J. Chem.* **2014**, *67*, 592-597.
(14) Dong, Y.; Qin, Y.; Dubaa, M.; Killion, J.; Gao, Y.; Zhao, T.; Zhou, D.; Duscher, D.; Geever, L.; Gurtner, G. C.; Wang, W. *Polym. Chem.* **2015**, *6*, 6182-6192.
(15) Undin, J.; Illanes, T.; Finne-Wistrand, A.; Albertsson, A. –C. *Polym. Chem.* **2012**, *3*, 1260-1266.
(16) Kesik, M.; Akbulut, H.; Söylemez, S.; Cevher, Ş. C.; Hızalan, G.; Udum, Y. A.; Endo, T.; Yamada, S.; Çırpan, A.; Yağcı, Y.; Toppare, L. *Polym. Chem.* **2014**, *5*, 6295-6306.
(17) Takara, M.; Toyoshima, M.; Seto, H.; Hoshino, Y.; Miura, Y. *Polym. Chem.* **2014**, *5*, 931-939.
(18) Engler, A. C.; Shukla, A.; Puranam, S.; Buss, H. G.; Jreige, N.; Hammond, P. T. *Biomacromolecules* **2011**, *12*, 1666-1674.
(19) Nederberg, F.; Zhang, Y.; Tan, J. P. K.; Xu, K.; Wang, H.; Yang, C.; Gao, S.; Guo, X. D.; Fukushima, K.; Li, L.; Hedrick, J. L.; Yang, Y. –Y. *Nat. Chem.* **2011**, *3*, 409-414.
(20) Fu, T. –H.; Li, Y.; Thaker, H. D.; Scott, R. W.; Tew, G. N. *ACS Med. Chem. Lett.* **2013**, *4*, 841-845.
(21) Al-Ahmad, A.; Laird, D.; Zou, P.; Tomakidi, P.; Steinberg, T.; Lienkamp, K. *PLoS One* **2013**, *8*, e73812.
(22) (a) Zhou, C.; Qi, X.; Li, P.; Chen, W. N.; Mouad, L.; Chang, M. W.; Leong, S. S. J.; Chan-Park, M. B. *Biomacromolecules* **2010**, *11*, 60-67; (b) Li, P.; Poon, Y. F.; Li, W.; Zhu, H. –Y.; Yeap, S. H.; Cao, Y.; Qi, X.; Zhou, C.; Lamrani, M.; Beuerman, R. W.; Kang, E. –T.; Mu, Y.; Li, C. M.; Chang, M. W.; Leong, S. S. J.; Chan-Park, M. B. *Nat. Mater.* **2011**, *10*, 149-156; (c) Li, P.; Zhou, C.; Rayatpisheh, S.; Ye, K.; Poon, Y. F.; Hammond, P. T.; Duan, H.; Chan-Park, M. B. *Adv. Mater.* **2012**, *24*, 4130-4137.
(23) Kolb, H. C.; Finn, M. G.; Sharpless, K. B. *Angew. Chem., Int. Ed.* **2001**, *40*, 2004-2021.
(24) Liang, L.; Astruc, D. *Coord. Chem. Rev.* **2011**, *255*, 2933-2945.
(25) Barner-Kowollik, C.; Du Prez, F. E.; Espeel, P.; Hawker, C. J.; Junkers, T.; Schlaad, H.; Van Camp, W. *Angew. Chem., Int. Ed.* **2011**, *50*, 60-62.
(26) Leriche, G.; Budin, G.; Brino, L.; Wagner, A. *Eur. J. Org. Chem.* **2010**, *2010*, 4360-4364.
(27) Yang, Y.; Song, X.; Yuan, L.; Li, M.; Liu, J.; Ji, R.; Zhao, H. *J. Polym. Sci. Part A: Polym. Chem.* **2012**, *50*, 329-337.
(28) Wong, E. H. H.; Lam, S. J.; Nam, E.; Qiao, G. G. *ACS Macro Lett.* **2014**, *3*, 524-528.
(29) McKenzie, T. G.; Fu, Q.; Wong, E. H. H.; Dunstan, D. E.; Qiao, G. G. *Macromolecules* **2015**, *48*, 3864-3872.
(30) McKenzie, T. G.; Wong, E. H. H.; Fu, Q.; Sulistio, A.; Dunstan, D. E.; Qiao, G. G. *ACS Macro Lett.* **2015**, *4*, 1012-1016.

(31) Zhao, C.; Patel, K.; Aichinger, L. M.; Liu, Z.; Hu, R.; Chen, H.; Li, X.; Li, L.; Zhang, G.; Chang, Y.; Zheng, J. *RSC Adv.* **2013**, *3*, 19991-20000.
(32) Vorobii, M.; de los Santos Pereira, A.; Pop-Georgievski, O.; Kostina, N. Y.; Rodriguez-Emmenegger, C.; Percec, V. *Polym. Chem.* **2015**, *6*, 4210-4220.
(33) Huesmann, D.; Birke, A.; Klinker, K.; Türk, S.; Räder, H. J.; Barz, M. *Macromolecules* **2014**, *47*, 928-936.
(34) (a) Blencowe, A.; Tan, J. F.; Goh, T. K.; Qiao, G. G. *Polymer* **2009**, *50*, 5-32; (b) Wong, E. H. H.; Blencowe, A.; Qiao, G. G. *Polym. Chem.* **2013**, *4*, 4562-4565; (c) McKenzie, T. G.; Wong, E. H. H.; Fu, Q.; Lam, S. J.; Dunstan, D. E.; Qiao, G. G. *Macromolecules* **2014**, *47*, 7869-7877.
(35) Gao, H.; Matyjaszewski, K. *Prog. Polym. Sci.* **2009**, *34*, 317-350.
(36) Wei, X.; Moad, G.; Muir, B. W.; Rizzardo, E.; Rosselgong, J.; Yang, W.; Thang, S. H. *Macromol. Rapid Commun.* **2014**, *35*, 840-845.
(37) Kuroda, K.; Caputo, G. A.; DeGrado, W. F. *Chem. Eur. J.* **2009**, *15*, 1123-1133.
(38) Saha, K.; Moyano, D. F.; Rotello, V. M. *Mater. Horiz.* **2014**, *1*, 102-105.
(39) Jindal, H. M.; Le, C. F.; Yusof, M. Y. M.; Velayuthan, R. D.; Lee, V. S.; Zain, S. M.; Isa, D. M.; Sekaran, S. D. *PLoS One* **2015**, *10*, e0128532.
(40) Ramamoorthy, A.; Thennarasu, S.; Tan, A.; Gottipati, K.; Sreekumar, S.; Heyl, D. L.; An, F. Y. P.; Shelburne, C. E. *Biochemistry* **2006**, *45*, 6529-6540.
(41) Zhu, W. L.; Nan, Y. H.; Hahm, K. –S.; Shin, S. Y. *J. Biochem. Mol. Biol.* **2007**, *40*, 1090-1094.
(42) Rotem, S.; Radzishevsky, I.; Mor, A. *Antimicrob. Agents Chemother.* **2006**, *50*, 2666-2672.
(43) Ruden, S.; Hilpert, K.; Berditsch, M.; Wadhwani, P.; Ulrich, A. S. *Antimicrob. Agents Chemother.* **2009**, *53*, 3538-3540.

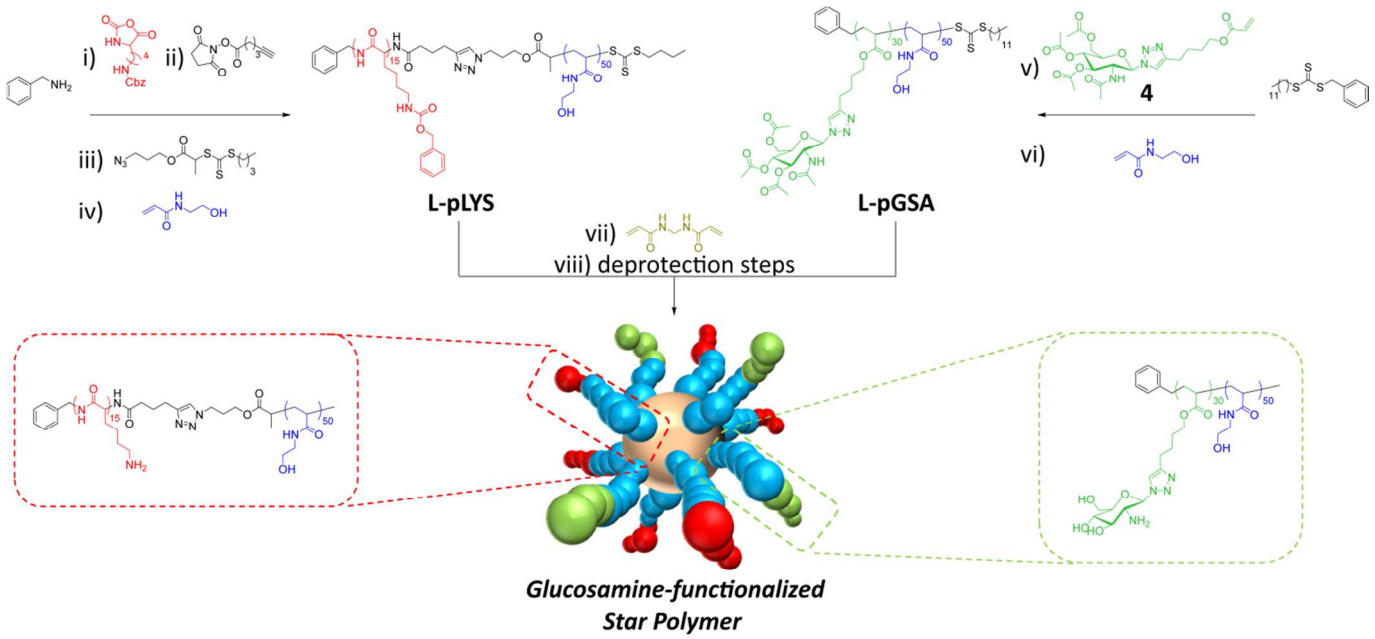

Scheme 1. Synthesis pathway for the formation of glucosamine-functionalized star polymers.

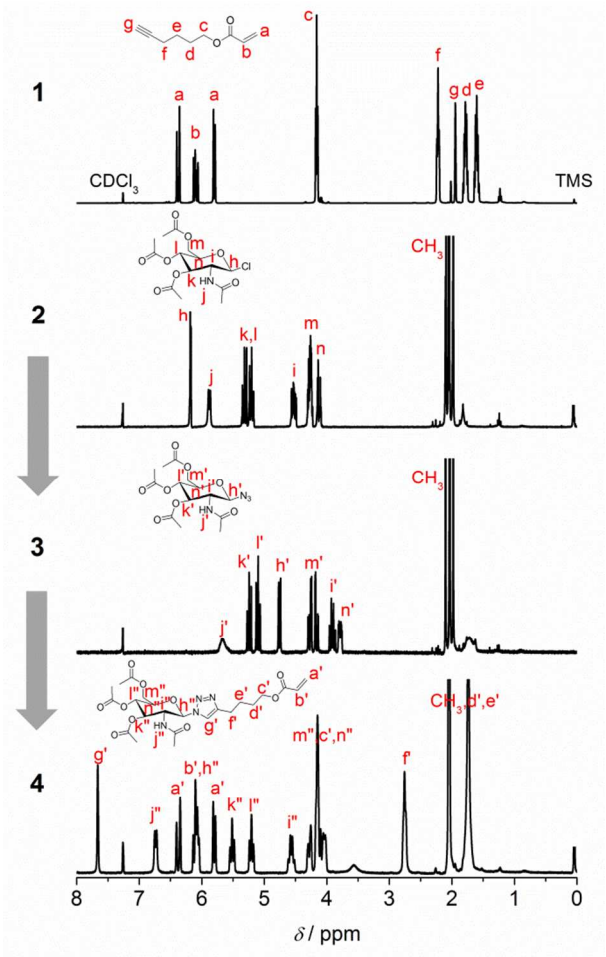

Figure 1. ^{1}H NMR spectra of the synthesized 5-hexynyl acrylate **1** as well as the sugar monomer precursors leading to the final acrylate-functionalized *N*-acetyl D-glucosamine peracetate monomer **4**.

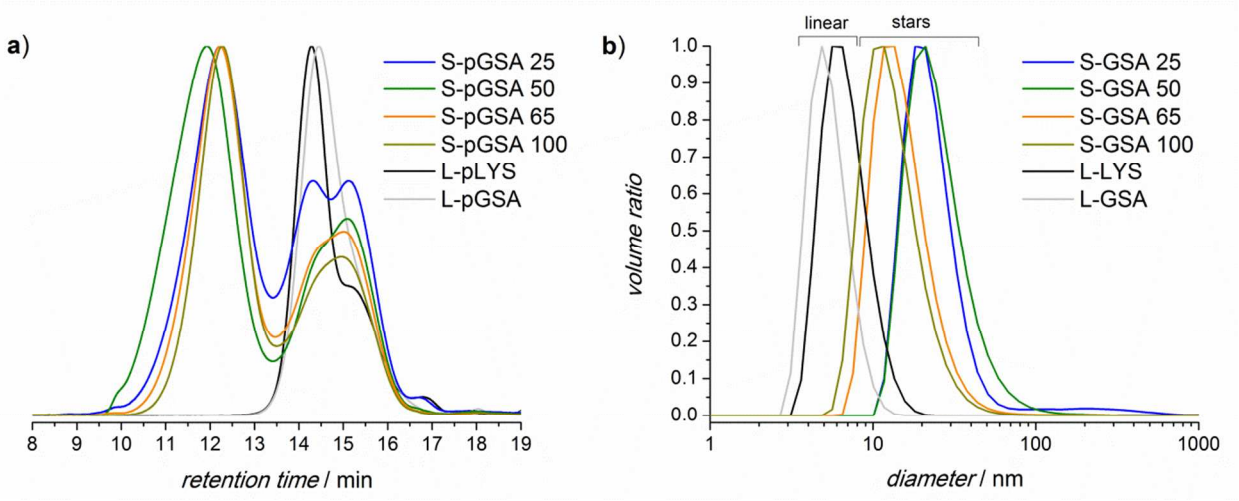

Figure 2. (a) GPC-DRI chromatograms of the protected macroinitiators and the corresponding (glucosamine-functionalized) star polymers prepared via the arm-first approach using RAFT-based photopolymerization. (b) DLS normalized volume distribution of the final deprotected forms as measured in water.

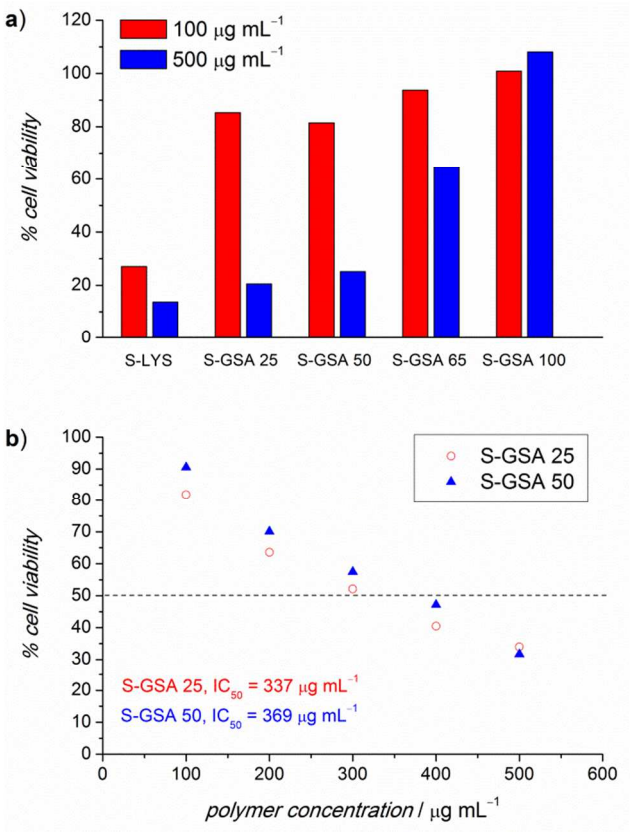

Figure 3. (a) Percentage of living AoSMC after 24 h incubation with various star polymers at sample concentrations of 100 and 500 μg mL^{-1}. (b) Determination of the SMC IC_{50} for S-GSA 25 and S-GSA 50. The horizontal dashed line indicates the cut-off point for 50% cell viability.

Table 1. Physical characterization of the macroinitiators and star polymers via GPC, DLS and zeta-potential analysis.

Entry	M_n[a] (g mol^{-1})	$Đ$[a]	% conv.[b]	N_{arm}[c]	d_H (nm)	ζ (mV)
S-GSA 25	168000	1.5	60	13	23.7	33.6
S-GSA 50	231000	1.7	65	19	25.9	33.4
S-GSA 65	167000	1.4	61	13	15.7	23.2
S-GSA 100	157000	1.3	63	12	13.7	8.3
L-LYS	13800	1.6	–	–	7.2	25.3
L-GSA	15200	1.4	–	–	5.5	1.2

[a]Determined based on the protected forms via a GPC-DMF system using narrow polystyrene standards as the reference. The M_n (and hence N_{arm}) values are relative to a polystyrene calibration and are estimates of the actual molecular weights. [b]Refers to the conversion of macroinitiator to star. [c]Estimated based on literature protocol.[34c]

Table 2. Antimicrobial and haemolytic activity as well as mammalian cell biocompatibility of glycosylated star polymers, and their comparison to other synthetic antimicrobial peptides.

Entry	MIC[a] (μg mL^{-1})						HC_{50} (μg mL^{-1})	IC_{50} (μg mL^{-1})	Selectivity[b]		Ref
	Gram-negative		Gram-positive						HC_{50}	IC_{50}	
	E. coli	*P. aeruginosa*	*S. aureus*	*MRSA*	*E. faecalis*	*VRE*	*RBC*	*SMC*	/MIC	/MIC	
S-LYS	32	256	16-32	16	8	32	> 10000	~ 0	> 417	~ 0	–
S-GSA 25	> 512	> 512	32-64	32	16	64	> 10000	337	> 208	7.0	–
S-GSA 50	> 512	> 512	64-128	128	64	256	> 10000	369	> 104	3.8	–
S-GSA 65	> 512	> 512	256	–	–	–	> 10000	610	> 39	2.4	–
S-GSA 100	> 512	> 512	> 512	–	–	–	–	–	–	–	–
L-LYS	64	256	16	–	–	–	–	~ 0	–	~ 0	–
L-GSA	> 512	> 512	> 512	–	–	–	–	–	–	–	–
Indolicidin	31.3	31.3	31.3	31.3	–	–	~ 250[c]	–	~ 8	–	[39]
Tachyplesin I	11.5	8.3	–	–	100	–	~ 340[c]	–	~ 41[d]	–	[40]
Melittin	2	2	0.5	–	–	–	~ 4[c]	–	~ 8	–	[41]
Magainin analog	1.5	–	9	–	–	–	45	–	5	–	[42]
Protegrin analog	3	–	3	–	–	–	9	–	3	–	[42]
Polymyxin B	1-2	–	–	–	–	–	~ 211[c]	–	~ 141[d]	–	[43]

[a]The strains used in this study were: *E. coli* (ATCC 8739), *P. aeruginosa* (ATCC 27853), *S. aureus* (ATCC 29213 and ATCC 25923), methicillin-resistant *S. aureus* (BAA-40), *E. faecalis* (OG1RF), vancomycin-resistant *E. faecalis* (V583). Note that some of the strains used for testing in this study differ from those used in the testing of other synthetic antimicrobial peptides listed in the table – please consult the appropriate references for the exact strains used. [b]Values were determined based on the MIC against *S. aureus*. [c]Extrapolated values. [d]Selectivity was determined using the lowest MIC value when no MIC values were recorded for *S. aureus*.

For Table of Contents Use Only

Modulating Antimicrobial Activity and Mammalian Cell Biocompatibility with Glucosamine-functionalized Star Polymers

Edgar H. H. Wong,†[a,b] Mya Mya Khin,[a,b] Vikashini Ravikumar,[c] Zhangyong Si,[a,b] Scott A. Rice[c,d] and Mary B. Chan-Park*[a,b]*